Catalysis Today 157 (2010) 351–358

Contents lists available at ScienceDirect

Catalysis Today

journal homepage: www.elsevier.com/locate/cattod

Production of acrolein and acrylic acid through dehydration and oxydehydration of glycerol with mixed oxide catalysts

J. Deleplanque[a,*], J.-L. Dubois[b], J.-F. Devaux[b], W. Ueda[c,*]

[a] Unité de Catalyse et de Chimie du Solide, Université Lille-Nord de France, Villeneuve d'Ascq, France
[b] Centre de Recherche Rhône Alpes, ARKEMA, Pierre Bénite, France
[c] Catalysis Research Center, Hokkaido University, Sapporo, Japan

ARTICLE INFO

Article history:
Available online 16 May 2010

Keywords:
Glycerol
Oxidative dehydration
Acrylic acid
Mixed oxide catalysts
Biomass

ABSTRACT

Dehydration of glycerol solution and further oxidation have been investigated with different mixed oxide catalysts. Among them, iron phosphates were found to be highly active and selective toward acrolein. Glycerol conversion was nearly complete and acrolein yields reach 80–90% after 5 h of test. Fresh and used catalysts were also characterized by different techniques (XRD, SEM, BET and TGA-DSC). Pure and well-defined structures were found more stable than relatively poor crystalline phase. Distribution of products changes during the deactivation of the catalyst, leading to by-products such as acetol, propanal and coke deposit on the surface of the catalyst, indicating a modification of the mechanism.

Introducing some oxygen in the feed allowed decreasing the amount of those by-products, but oxidation products appeared such as acetic acid or CO_x on detriment of the yield in acrolein. Using appropriate mixed oxide catalysts such as molybdenum/tungsten vanadium based catalysts showed interesting performances to obtain acrylic acid directly from glycerol.

1. Introduction

As crude oil resources will be exhausted in a few decades, renewable resources as alternative raw materials for intermediates are becoming more and more studied. Among them, we recently observed a renewed interest in the conversion of biomass and biomass-derived products into fuels and chemicals, because the processing of biomass is CO_2 neutral [1–4]. Acrolein is an important intermediate for the chemical industry, in order to produce acrylic acid esters, methionine, fragrances, polymers or detergents. The actual industrial process to obtain acrolein is the gas phase oxidation of propylene with a Bi/Mo-mixed oxide catalyst. Selectivity in acrolein can reach 85% with a propylene conversion of 95% [5]. Such oil derived process suffers from a great dependency on oil prices and the use of propylene directly contributes to the large amount of carbon dioxide emitted by industries in the atmosphere. As an alternative way, acrolein can be produced by the dehydration of glycerol, which appears as by-product produced in a large amount during biodiesel production.

Indeed, Scheering-Kahlbaum proposed a patent in 1933 dealing with the dehydration of glycerol in the gaseous phase over supported lithium-phosphate catalyst or copper-phosphate catalyst at temperature between 573 and 873 K [6] and yield in acrolein could reach 75%. More recently, several groups [7–14] have studied glycerol dehydration in the gas phase, liquid phase or even supercritical phase over solid acid catalyst such as zeolites, phosphates, sulfates, heteropolycompounds and metal oxides. A recent review by Dumeignil et al. [15] summarizes results obtained in the literature. These studies generally conclude about the role of acidity and porous structure of catalysts. However, deactivation of catalyst and high amount of by-products were always observed by these authors.

Arkema Company proposed a solution in order to prevent catalyst from deactivation by using oxygen or air in the feed during the dehydration reaction [16,17]. Oxygen adding can avoid the formation of coke by burning and may have a positive effect on reducible catalyst since glycerol is considered as a strong reductant. Our group also worked on oxygen-containing feeds on VPO catalysts which could convert 100% glycerol to obtain 66% selectivity to acrolein and 14% selectivity to acetaldehyde [18]. Using oxygen could decrease the amount of by-products, inhibit coke formation and keep the catalyst in its oxidized state. The structure of VPO catalyst remained stable during the reaction. 8% Acrylic acid yield could be observed with oxygen-rich feed at higher temperature (623 K).

The goal of this study is to develop a one-step process to obtain acrylic acid directly from glycerol by oxydehydration. Such process could be economically interesting because it would reduce engineering investment. The other point is that heat balance may

* Corresponding author. Tel.: +81 11 706 9164; fax: +81 11 706 9164.
E-mail addresses: jeremy.deleplanque@neuf.fr (J. Deleplanque), ueda@cat.hokudai.ac.jp (W. Ueda).

0920-5861/$ – see front matter © 2010 Elsevier B.V. All rights reserved.
doi:10.1016/j.cattod.2010.04.012

be reached with the endothermic character of dehydration and exothermic character of oxidation. Iron phosphate catalysts are known to be good catalysts for the oxidative dehydration of isobutyraldehyde to methacrolein or lactic acid to pyruvic acid [19–22]. Also, molybdenum vanadium based catalysts are active and selective for the partial oxidation of propane to acrylic acid or acrolein to acrylic acid [23–29]. These catalysts were synthesised and tested in dehydration and oxydehydration of glycerol in the gas phase. Effect of structure and oxygen is discussed herein and possible reaction mechanism is proposed.

2. Experimental

2.1. Synthesis of the catalysts

All reagents were analytical grade, purchased from Wako Pure Chemical Industries, Ltd., and used without further purification. Phosphotungstic acid ($H_3PW_{12}O_{40}\cdot 13H_2O$) was provided by Kanto Chemicals and used as received without any purification. Q10 silica was provided by CARiACT. Heating rates of calcinations procedure were fixed to 10 K min^{-1}.

Iron (III) phosphate catalysts were prepared by four different methods. The first method, called the ammonia method (FeP-A), was previously described by Mamoru Ai [19–21]. 12.41 g of $(Fe)NO_3\cdot 9H_2O$ was dissolved in 500 mL of water and diluted 4.53 g of NH_3 (28 wt%) was added to the solution in order to obtain an Iron hydroxide gel. The obtained precipitate was filtered, washed and mixed with 3.10 g of 85% orthophosphoric acid solution H_3PO_4 to obtain a P/Fe ratio of 1.2. The paste-like compound was then dried at 400 K for a night and calcined under a flow of air (30 mL min^{-1}) at 673 K for 5 h.

The ammonia hydrothermal method was derived from the previous one. Water was added to the mixture of Iron hydroxide gel and orthophosphoric acid (P/Fe = 1) and the final solution was stirred and put in a stainless steel autoclave fitted with a Teflon inner vessel. The autoclave was heated at 450 K during 70 h. After filtration, drying and calcinations procedure was the same as those for the previous method. The catalyst was named FeP-AH.

For the precipitation–concentration method (catalyst denoted FeP-P), the synthesis was already described by Millet [22]. 12.29 g of $Fe(NO_3)\cdot 9H_2O$ was dissolved in 500 mL of water and 4.03 g of orthophosphoric acid (P/Fe = 1.15) was added under stirring and heating at 353 K until evaporation. The obtained powder was dried at 350 K and finally calcined under air at 773 K during 6 h. The last preparation of iron phosphate catalyst was done by hydrothermal synthesis. An equimolar amount (0.17 mol) of $FeCl_3\cdot 6H_2O$ and 85% H_3PO_4 were diluted in 200 mL of water under stirring and put in a 300 mL stainless steel autoclave. The Autoclave was heated at 423 K during 14 h. The resulted pink solid was dried one night at 353 K and calcined at 673 K under air (30 mL min^{-1}) during 4 h. Catalyst was denoted FeP-H.

Molybdenum vanadium based catalysts were prepared hydrothermally by the method usually used in the laboratory and their synthesis has been reported elsewhere [23–27]. In details, an amount of 8.82 g of $(NH_4)_6Mo_7O_{24}\cdot 4H_2O$ was dissolved in 120 mL of distilled water. Separately, an aqueous solution of vanadium was prepared by dissolving 3.28 g of $VOSO_4\cdot nH_2O$ (MITSUWA Chemicals, assay 62%) in 120 mL of distilled water. The two solutions were mixed at 293 K and stirred for 10 min before being introduced into the stainless steel autoclave equipped with a 300 mL Teflon inner tube. The concentration of Mo in the mixed solution (dark purple liquid) was 0.2 mol L^{-1}. Hydrothermal reaction of the liquid (mole ratio: Mo/V = 1/0.25) was carried out for 20 h. Gray solids were yielded in the bottom of the autoclave as well as on the wall. The obtained solid was separated from the solution, washed with distilled water, and dried at 353 K over night. Dried solid was calcined at 673 K under a flow of nitrogen (50 mL min^{-1}) during 4 h.

Tungsten vanadium oxide was prepared as follows: 10 g of $(NH_4)_6[H_2W_{12}O_{40}]\cdot nH_2O$ ammonium tungstate metahydrate was dissolved in 120 mL water. The second solution was prepared by adding 3.3 g of $VOSO_4\cdot nH_2O$ (MITSUWA Chemicals, assay 62%) in 120 mL of water. The two solutions were mixed under stirring during 10 min before being introduced into a 300 mL autoclave. The mixture was deaerated by nitrogen bubbling and the autoclave was then heated at 448 K for 73 h. The solid was filtered out and washed with water. The filtrate was dried at 353 K for 24 h and pretreated at 673 K in air (50 mL min^{-1}) for 2 h and 813 K (80 mL min^{-1}) in nitrogen for 2 h.

2.2. Characterizations

The powder XRD patterns were recorded on a diffractometer (Rigaku, RINT Ultima+) with CuKα radiation (wavelength λ = 1.54056 Å). Scanning electron microscopy field emission scanning electron microscopy (FE–SEM) was performed on a JSM-7400F (JEOL). Specific surface areas were measured by N_2 adsorption at 77 K using BET method over Autosorb 6AG (Quantachrome Instruments). The measurements of thermogravimetric-differential thermal analysis (TG-DTA) were performed on a TG-8120 (Rigaku) thermogravimetric analyzer. Dry air or N_2 provided by a pressure tank with a flow rate of 30 mL min^{-1} was used as the carrier gas.

Acidity of catalysts was measured by titration using Hammet indicators and NH_3-TPD. Hammet indicators were dimethylaminoazobenzene (pK_a = +3.3), benzeneazodiphenylamine (pK_a = +1.5), dicinnamalacetone (pK_a = −3.0), p-benzalacetophenone (pK_a = −5.6) and anthraquinone (pK_a = −8.2). Temperature-programmed desorption (TPD) of ammonia, NH_3-TPD, was employed to measure oxide surface acidity. The experiment was carried out on a BELSORP apparatus. The catalyst (ca. 100 mg) was pre-heated under helium at 573 K for 1 h. Then, ammonia was introduced at 373 K for 30 min. Desorption profile and temperature-programmed decomposition mass spectrometry (TPD-MS) measurements were performed from 393 to 873 K at a heating rate of 10 K min^{-1} in helium flow. The decomposed gas molecules were monitored by a mass spectrometer (ANELVA, Quadrupole Mass Spectrometer, M-100QA, BEL Japan).

2.3. Catalytic tests

Catalytic oxydehydration in gas phase was carried out at an atmospheric pressure in a conventional flow system with a fixed bed Pyrex tubular reactor (420 mm length × 8 mm inside diameter). Catalyst were crushed and sieved before test (125–200 μm) mixed with quartz sand (50–80 mesh) and initially pretreated at 573 K in a flow of nitrogen (30 mL min^{-1}) for 2 h. Glycerol solution was composed by 40 wt% of glycerol in water and was introduced in the flow of nitrogen and oxygen with help of syringe pump at a flow of 0.48 g h^{-1}. The feed compositions, the total flow rates of the mixed reactant gases, and the amount of the catalysts used were shown in the footnote of the tables. Products were collected after the reactor in a cold trap. The concentrations of products obtained in the liquid phase were measured by gas chromatography mass spectrometry (GC–MS) using a flame ionization detector (Shimadzu Classic–5000, TC WAX column 60 m, 0.25 mm, 0.25 μm). Inlet and outlet gas phase (including entrapped products) were analyzed with three on-line gas chromatographs with columns, Molecular Sieve 13X, Gaskuropack 54 and Porapak Q. This GC system allowed the quantification of nitrogen, oxygen, CO, CO_2, acrolein, acetaldehyde and acetic acid. Quantities of products were deduced from the amount of nitrogen, assuming that nitrogen flow is constant. Analyses of

Table 1
Catalytic results over $H_3PW_{12}O_{40}$ and the four iron phosphate catalysts at 353 K.

Catalysts	$H_3PW_{12}O_{40}$	$FePO_4$			
		FeP-A	FeP-AH	FeP-P	FeP-H
Glycerol conversion	100.0	100.0	97.7	100.0	100.0
Carbon balance	88.2	85.1	87.6	91.0	96.5
Acrolein	76.6	78.4	81.5	85.3	92.1
Acetaldehyde	0.6	0.8	0.1	1.0	1.3
Hydroxyacetone	1.0	0.0	2.7	0.0	0.0
Propanal	0.2	0.2	0.0	0.9	0.1
Others	9.8	5.7	3.3	3.8	3.0

Conversion (%) and yield (%). Reactions conditions: 0.8 g of catalyst diluted in 1.0 g of quartz sand (except for $H_3PW_{12}O_{40}$ 2.0 g in 2.0 g of quartz). Aqueous solution of glycerol (40 wt%). Feed composition vol.% [$N_2/H_2O/Gly$] = [46/48/6]. GHSV = 600 h^{-1} (1230 h^{-1} for $H_3PW_{12}O_{40}$). Total flow rates, 20 mL min^{-1}. Others contain formaldehyde, acetone, 2-propen-1-ol, phenol, formic acid, propanoic acid, acrylic acid and other cyclic-ether products identified as 1,3-dioxan-5-ol, 4-methanol-1,3-dioxolane and 2-ethylenyl-4-methanol-1,3-dioxolane. Unknown products are included in the missing carbon.

both liquid phase and gas phase were summed in order to calculate glycerol and oxygen (when required) conversion, selectivity and mass balance. Carbon balance (%) was obtained by summing up the remained glycerol and the total amount of detected and quantified products in the liquid phase and in the gas phase.

3. Results and discussion

3.1. Dehydration of glycerol

3.1.1. Catalytic results

Table 1 presents results obtained in the dehydration of glycerol at 553 K after 5 h of catalytic test for phosphotungstic acid and the four iron phosphate catalysts. Glycerol is completely converted in most of the cases and acrolein is the main product. The five catalysts present similar performances but few differences can be observed. Indeed, the amount of by-products is slightly different for those catalysts. Yields in acrolein overreach 70% in every case and more than 90% with iron phosphate prepared by hydrothermal method (FeP-H). As a consequence, by-products obtained with this last catalyst are very low and the main by-product is acetaldehyde. Except for FeP-AH which produces more hydroxyacetone (2.7%), the main differences between those catalysts are the amount of by-products. GC–MS analysis and mass spectral database were necessary to identify some compounds. Those products resulting from acetalization, reactions which happen in an acidic environment and usually in acidic solution, are formed by the reaction of glycerol and formaldehyde (to produce 1,3-dioxan-5-ol), acetaldehyde (1,3-dioxolane-4-methanol) or acrolein (1,3-dioxolane-4-methanol, 2-ethylenyl-). The highest amount of such by-products was observed with phosphotungstic acid $H_3PW_{12}O_{40}$. As non-supported Keggin type heteropolyacids are water-soluble, cyclic-ether by-products can be formed after the catalytic bed in the solution acidified by the solubilised $H_3PW_{12}O_{40}$. However, some compounds are still unknown and are included in the missing carbon.

Fig. 1 presents the evolution of conversion of glycerol and distribution of products for the four iron phosphate catalysts with time on stream. Phosphotungstic acid could not be compared due to fast drop of carbon balance. Stability seems to depend on the preparation method of the catalyst.

Drop in the glycerol conversion (Fig. 1b–d), in the selectivity in acrolein (Fig. 1a–c) or change in the distribution of products imply a modification of the mechanism and deactivation of the catalyst. Modification of the mechanism can be observed by an increasing amount of by-products such as hydroxyacetone, acetaldehyde or propanal. We suppose there is a modification of active sites during the reaction, inducing other routes to obtain those by-products. Deactivation can also be observed as carbon balance is decreasing with time on stream (not shown). Missing carbon is actually due to an increase amount of unknown molecules and carbon deposit on the surface of catalysts.

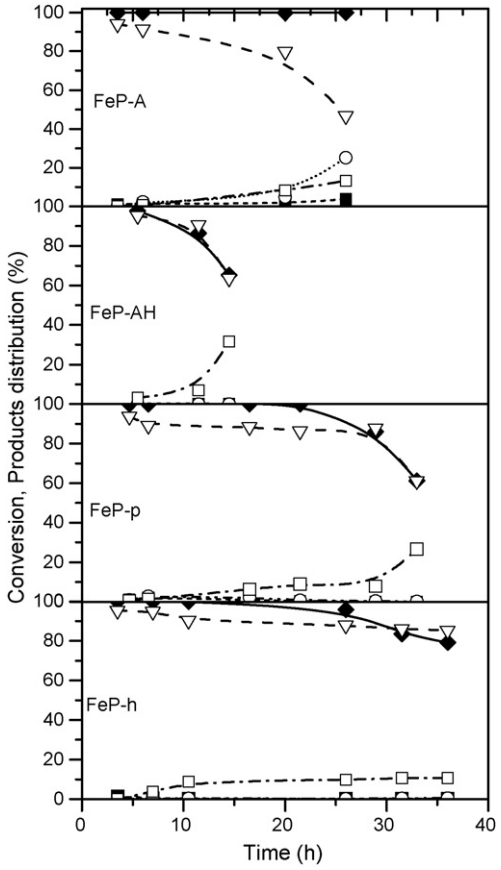

Fig. 1. Catalytic performances of iron phosphate catalysts with time on stream. Glycerol conversion ( ), and selectivity in acrolein (▽), hydroxyacetone ( ), acetaldehyde ( ) and propanal (◯).

As observed in Fig. 1a–d, stability of catalysts greatly depends on the preparation method of the catalyst. Few parameters were studied in the literature in order to explain the performances of various catalysts. Among them, acidity and textural properties were discussed [7–11,14,15]. Particularly, Chai et al. [9] compared acid-base catalysts classified in different groups depending on their acidity. Authors showed that very strong acid catalysts ($H_0 \leq -8.2$) are more active than strong acid catalysts ($-8.2 \leq H_0 \leq -3$) but less selective toward acrolein due to the severe coking of the catalysts. Weak acid catalysts ($-3 \leq H_0 \leq +6.8$) presented the lowest yields in acrolein whereas solid base catalysts are not effective for the dehydration of glycerol into acrolein. Catalysts with large pores (>10 nm) such as Al_2O_3–PO_4 or TiO_2–PO_4 exhibit high activity in the dehydration of glycerol but limited selectivity toward acrolein. On the other hand, small micropores (0.5–0.6 nm) were less active but more selective [14]. Same conclusions about the lower activity of smaller pore size were brought by Tsukuda et al. [7], excepted that the size they mentioned were fairly higher (3–6 nm). Thus, activity in the dehydration of glycerol and selectivity toward acrolein seem to depend both on acid strength and pore size.

3.1.2. Influence of acidity and textural properties

Phosphotungstic acid ($H_3PW_{12}O_{40}$) is well-known as a pure and strong Brönsted acid with a Hammet acidity of $H_0 < 12$ but its sur-

Table 2
BET specific surface area and NH_3-TPD results of iron phosphate catalysts.

Preparation method	Surface area ($m^2\,g^{-1}$)	NH_3-TPD	
		Temperature of maximum desorption (K)	Desorbed amount ($\mu mol\,g^{-1}$)
FeP-A	43.6	461	1939
FeP-AH	2.6	–	–
FeP-P	7.8	435	95
FeP-H	8.7	449	45

face specific area is relatively low ($5\,m^2\,g^{-1}$). To increase surface area, we prepared and tested a 30% $H_3PW_{12}O_{40}/SiO_2$ catalyst by supporting $H_3PW_{12}O_{40}$ on CARiACT Q10 silica by incipient wetness impregnation. Compared to bulk $H_3PW_{12}O_{40}$, stability can only be slightly enhanced using silica support as deactivation (drop in acrolein yield and carbon balance) can be observed after 10–15 h of test. Acrolein selectivity was 65% with a carbon balance of 72% after 15 h of test (data not shown). However, stability is still lower than those observed with iron phosphate catalysts. Actually, the amount of HPW supported on silica (30 wt%) is probably too important, leading to the presence of bulk $H_3PW_{12}O_{40,}$ strong acidic materials. These conclusions were already exposed in the literature by Atia et al. [11].

On the contrary, iron phosphate catalysts are not known to be strong acidic catalysts. Titration showed that these catalysts have a Hammet acidity of $-3 < H_0 < +1.5$. Table 2 summarizes surface specific area and acidic properties obtained by NH_3-TPD with the four iron phosphate catalysts and Fig. 2 presents ammonia desorption profiles for these catalysts. FeP-A presents a specific surface area of $43.6\,m^2\,g^{-1}$, higher than FeP-P and FeP-H ($7.8\,m^2\,g^{-1}$ and $8.7\,m^2\,g^{-1}$, respectively) and FeP-AH ($2.6\,m^2\,g^{-1}$). NH_3-TPD results confirm the weak acidity of the catalysts with a temperature of maximum desorption included between 435 and 461 K. Without any detected desorbed ammonia and presenting the lowest surface area, FeP-AH presents the lowest density of acid sites which can explain the presence of hydroxyacetone after only 5 h of test and a faster drop in conversion. On the opposite, FeP-A, the "strongest" acid (temperature of maximum desorption of 461 K) with the highest acid sites density also deactivated quite fastly. The most obvious proof of FeP-A's deactivation is a rapid drop of carbon balance and acrolein yield. This should indicate a higher coke deposit on the surface of the catalyst and thus, production of H_2 which can react with acrolein to form propanal or 2-propen-1-ol. With an intermediate

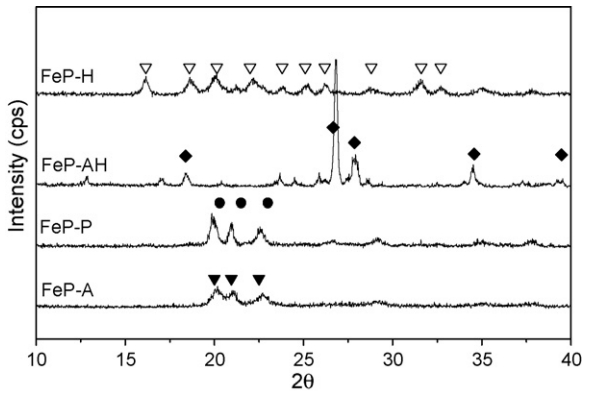

Fig. 2. TPD spectra of ammonia adsorbed on iron phosphate catalysts.

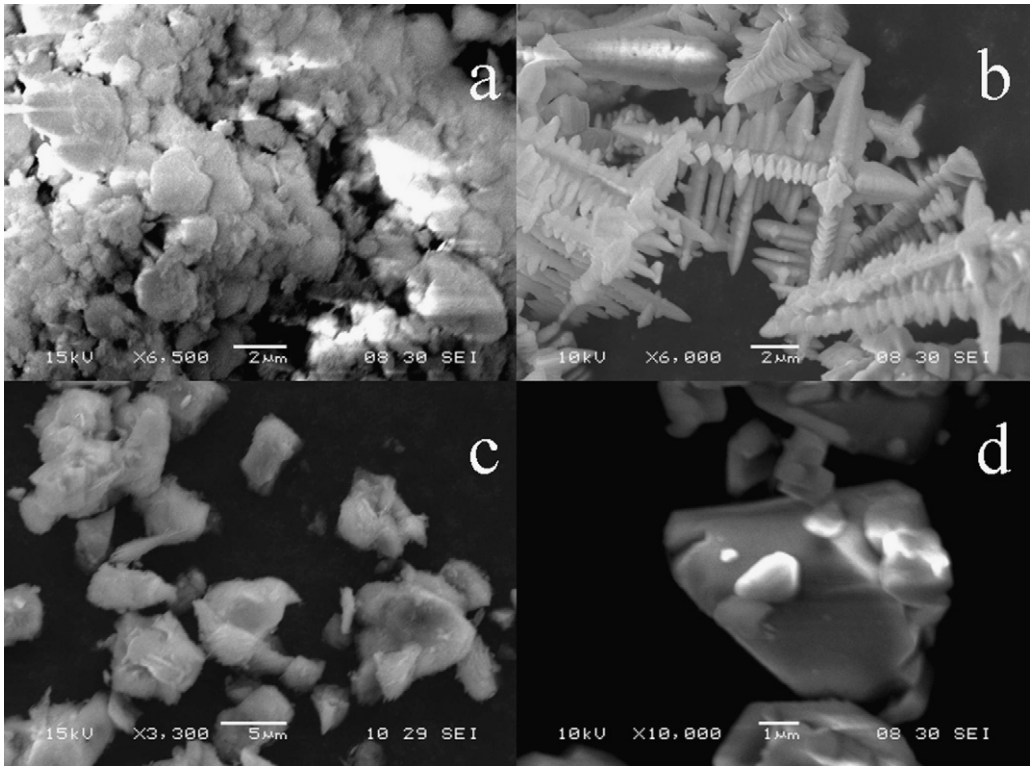

Fig. 3. XRD patterns iron phosphate catalysts. (▼) = $FePO_4$ (X-phase) XRD peaks, (●) = $FePO_4$, tridymite structure, ( ) = $Fe_5(PO_4)_4(OH)_3$ XRD peaks and (▽) = monoclinic $FePO_4$ XRD peaks.

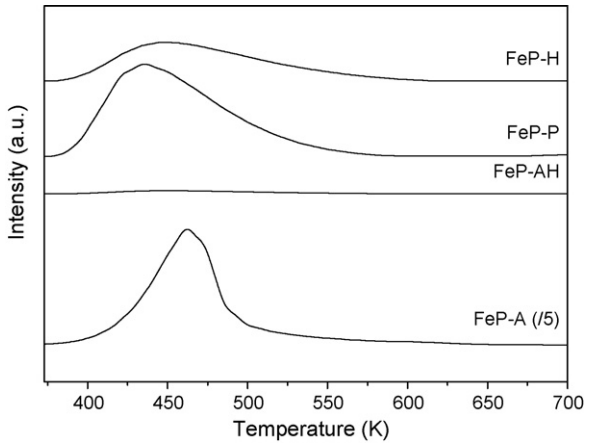

Fig. 4. SEM images of (a) FeP-A, (b) FeP-AH, (c) FeP-P and (d) FeP-H.

acidity both in strength and density, stability is improved with FeP-P and FeP-H. In the first 5 h, acidity is strong enough to avoid the formation of hydroxyacetone (loss of one molecule of water) but not too strong to prevent coke formation.

Thus, acidity is an important parameter for the dehydration of glycerol to form acrolein. However, even weak acidic catalysts can perform the reaction with the advantage of avoiding, or at least, decreasing coke formation of the surface of the catalyst.

3.1.3. Influence of structure and morphology of the catalysts

Figs. 3 and 4 present the XRD patterns and the SEM images of the synthesised iron phosphates, respectively.

Iron phosphate prepared by the ammonia method (FeP-A) whose XRD patterns is characterized with three main peaks at $2\theta = 20.0^\circ$, 21.0°, and 22.5° (Fig. 3a), was already described as the X-phase by Ai et al. [19] and identified later as the tridymite-like phase by the same authors [20,21]. As observed in Fig. 3a and 4a, these catalysts showed a relatively poor crystalline structure and an amorphous-like morphology with particles size of ca. 4–16 μm^2. Tridymite-like structure is also obtained for the catalyst prepared by the precipitation–concentration method (FeP-P), with a fairly more crystallised structure (Fig. 3c) and defined crystals of ca. 20 μm^2 (Fig. 4c). However, the purer Tridymite phase obtained with the precipitation–concentration method is due to P/Fe ratio closer to 1.

Using the hydrothermal synthesis starting from the ammonia method (FeP-AH) led to a well-crystallised giinite phase $Fe_5(PO_4)_4(OH)_3$ (Fig. 3b). Hydroxyl groups observed in this catalyst are due to the addition of water needed for the hydrothermal synthesis. Shapes of particles are completely different through this preparation method as the catalyst presents a spinal morphology of 12–15 μm length (Fig. 4b). This spinal morphology confirms the low specific surface area of FeP-AH (2.6 $m^2\ g^{-1}$).

Iron phosphates prepared by hydrothermal synthesis starting from the iron (III) chloride (FeP-H) present a pure phosphosiderite (monoclinic) structure of $FePO_4{\cdot}2H_2O$ (not shown) which leads to a pure monoclinic phase $FePO_4$ (Fig. 3d) after treatment at 473 K, stable until 873 K [28] and possess some well-shaped crystals with relatively flat and large surfaces of 25 μm^2 (Fig. 4b).

Acidity is known in the literature as an important parameter for the dehydration of glycerol [8–11,14,15]. Nevertheless, structure seems to have an effect also on the stability of the catalyst. Our two best iron phosphate catalysts (FeP-P and FeP-H) present relatively well-shaped particles with large and flat surfaces (Fig. 4c and d). FeP-H, with a well-crystallised structure, slightly more defined particles with larger surfaces, is the most stable iron phosphate catalyst we synthesised and tested. As a consequence, we can assume that structure have also an effect on the distribution and stability of catalyst in the dehydration of glycerol. However, deactivation is a key step in this reaction and coke is always observed on the surface of the catalyst even with weak acidic solid. Previous reports [18] showed that the use of oxygen could prevent catalyst from coking. We discuss that point with our catalysts in the next part.

3.1.4. Effect of oxygen

A catalytic test with FeP-H and a 40% glycerol solution was conducted with addition of oxygen in the gas flow. The composition of the feed was vol.% [$N_2/O_2/H_2O$/glycerol] = [23/8/61/8] and the gas hourly space velocity was 600 h^{-1}. Table 3 summarizes results obtained with that experiment. Glycerol conversion was 100%, oxygen conversion 48% and 72% at 553 and 573 K, respectively and the main product was acrolein. Obviously, the use of oxygen had a positive effect on the amount of by-products, as hydroxyacetone was absent from the reaction products. However, selectivity in acetaldehyde and acetic acid increased and some new by-products arose such as CO and CO_2. As a consequence, oxygen had a negative effect on selectivity in acrolein, which dropped to 62.5%. Rising the temperature to 573 K led to a worse trend where selectivity on by-products (acetic acid, acetaldehyde, CO and CO_2) increased on detriment of selectivity in acrolein.

Anyway, the main product is still acrolein. We could initially expect that the addition of oxygen would help to oxidize acrolein into acrylic acid, but yields in acrylic acid could not reach more than 1.2%. Thus, iron phosphate catalysts are not good candidates for the direct oxydehydration of glycerol into acrylic acid, certainly due to the single bonds Fe–O and P–O.

3.2. Oxydehydration of glycerol

Molybdenum vanadium based catalysts, known as active and selective in the partial oxidation of propane or acrolein into acrylic acid [23–26] were studied in the oxydehydration of glycerol. We used the most active catalyst in those reactions, MoVTeNbO, and also Mo_3VO successfully synthesised in its orthorhombic phase in the laboratory. We also succeeded to hydrothermally synthesise a new W_3VO catalysts with a pseudo-hexagonal like phase.

3.2.1. Characterization of catalysts

Fig. 5 presents XRD patterns of our synthesised molybdenum/tungsten vanadium based catalysts and Fig. 6 shows the SEM images of MoVTeNbO and W_3VO catalysts. MoVTeNbO and Mo_3VO catalysts with their orthorhombic structure were previously described in the literature [23–27]. These crystalline structures consist of five MoO_6 octahedrons surrounding one MoO_7

Table 3
Effect of oxygen and temperature on catalytic results over FeP-H catalysts.

Temperature	X_{GLY}	X_{OXY}	CB	ACR	ACE	HYD	FoA	PrA	AA	AcA	CO	CO_2	Ethers
553 K	100	48.0	83.3	62.5	2.3	0.0	0.6	1.2	0.5	3.3	4.7	8.2	0.0
573 K	100	72.3	80.4	50.7	3.8	0.0	0.2	0.1	1.2	3.8	8.2	11.3	0.0

Reactions conditions: 1.3 g of catalyst diluted in 1.5 g of quartz sand. Feed composition vol.% [$N_2/O_2/H_2O$/Gly] = [23/8/61/8]. GHSV = 550 h^{-1}. Conversions – X_{GLY}: glycerol, X_{OXY}: oxygen; CB: carbon balance; yields – ACR: acrolein, ACE: acetaldehyde, HYD: hydroxyacetone, FoA: formic acid, PoA: propanoic acid, AA: acrylic acid, AcA: acetic acid.

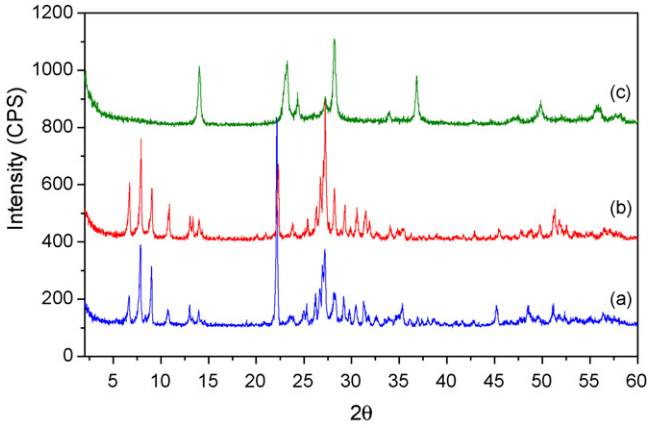

Fig. 5. XRD patterns of (a) Mo_3VO, (b) MoVTeNbO and (c) W_3VO.

pentagonal bi-pyramid by edge-sharing. The six or seven member rings formed by these connections are interconnected with MoO_6 or VO_6 by corner-sharing [27]. Tellurium, previously thought to be necessary to obtain the orthorhombic structure, is located on the hexagonal channels of the orthorhombic Mo–V–O and can enhance the thermal stability of the structure [24]. These catalysts form rodlike crystals with lengths of up to several tens of micrometers (Fig. 6) [27]. Vanadium tungsten oxide presents similar rodlike crystals (Fig. 6) but different XRD patterns (Fig. 5c). This structure can be characterized as pseudo-hexagonal structure as XRD patterns is really close to the one obtained for the MoVSbO M2 phase described previously [29]. Discussion upon this structure will be published elsewhere.

3.2.2. Catalytic results

Starting from the same 40 wt% glycerol solution, oxygen was added to the feed in order to obtain the following composition vol.% [$N_2/O_2/H_2O$/glycerol] = [72/6/19/3] and the gas hourly space velocity was 2800 h^{-1}. Table 4 presents the results obtained with those catalysts after 5 h of time on stream. Carbon balances were included between 95% and 105% in every cases and oxygen balances upper than 85%.

As observed in the experiment without oxygen, glycerol conversion is complete or nearly complete. Oxygen conversions were included between 66% and 75%. Glycerol is known to be a strong reductant at high temperature reactions and metal centers with high valences can easily undergo reduction. Thus, these levels of oxygen conversion are low enough to prevent catalyst from reduction. The desired product, acrylic acid could reach fairly good yield of 23.7% with W_3VO, 26.3% with Mo_3VO and 28.4% with MoVTeNbO. Remained yields in acrolein were very low (between 0% and 3%) indicating a nearly complete oxidation of it, especially with W_3VO.

Nevertheless, we usually produced as much acetic acid as acrylic acid and a large amount of other oxidation products CO and CO_2. We previously observed an increase in the acetaldehyde yield in the presence of oxygen with iron phosphate catalysts which can explain why acetic acid yield is so high with molybdenum/tungsten vanadium based catalysts. Oxidation of acrolein into acrylic acid with Mo_3VO catalysts did not produce so much acetic acid at 500 K [24]. But we can suppose that the amount of acetic acid increases at higher temperatures and that a part of acetic acid and CO_x come from the oxidation of acrolein, as previously proposed by our group [18]. This leads to the same conclusion that adding oxygen in the feed modifies the mechanism of glycerol dehydration and thus, of further oxidation.

The new structure W_3VO does not produce as by-products (formic acid and propanoic acid) as Mo_3VO and MoVTeNbO. Indeed, those products resulting from the oxidation of formaldehyde and propanal, respectively, were detected only with molybdenum based catalysts. Same observations were done concerning the cyclic-ether products formed by formaldehyde addition to glycerol, 1,3-dioxan-5-ol and 1,3-dioxolane-4-methanol. Formaldehyde is supposedly formed with acetaldehyde during the 1,3 dehydration of glycerol [30]. As acetic acid is produced on a large amount with W_3VO, acetaldehyde is surely formed during the dehydration step of glycerol. Also, W_3VO produces more CO_2 than molybdenum based catalysts and as CO as MoVTeNbO. We can propose that formaldehyde is directly oxidized into CO and CO_2 with W_3VO, catalyst which also oxidize more acrolein.

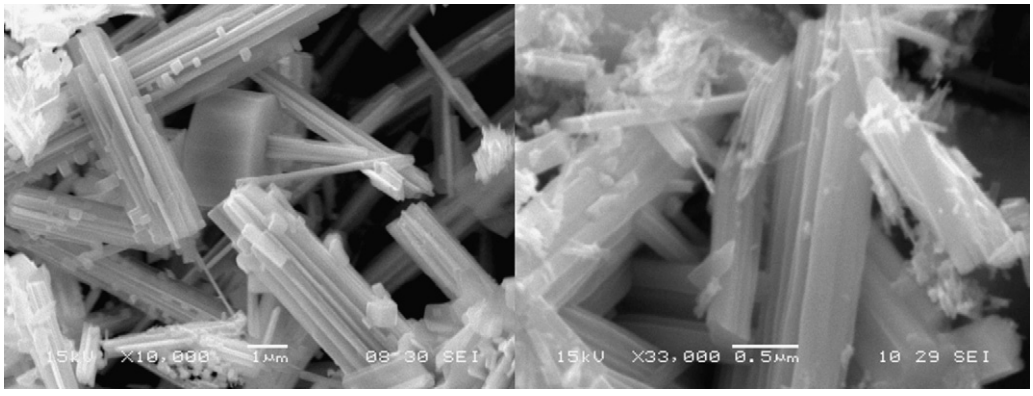

Fig. 6. SEM images of MoVTeNbO (left) and W_3VO (right).

Table 4
Oxydehydration of glycerol with molybdenum/tungsten vanadium based catalysts.

Catalyst	X_{GLY}	X_{OXY}	ACR	ACE	HYD	FoA	PrA	AA	AcA	CO	CO_2	Ethers
Mo_3VO	100	72.0	3.0	0.9	0.0	4.0	1.7	26.3	23.5	18.1	17.0	3.4
MoVTeNbO	99.6	75.6	1.7	0.1	0.0	2.7	2.8	28.4	23.2	29.7	15.1	3.8
W_3VO	100	66.0	0.1	0.0	0.0	0.0	0.0	23.7	23.2	28.3	26.4	0.0

Reactions conditions: 0.3 g of catalyst diluted in 0.3 g of quartz sand. Feed composition vol.% [$N_2/O_2/H_2O$/Gly] = [72/6/19/3]. GHSV = 2800 h^{-1}. Total flow rates, 36 mL min^{-1}. Conversions – X_{GLY}: glycerol, X_{OXY}: oxygen, yields – ACR: acrolein, ACE: acetaldehyde, HYD: hydroxyacetone, FoA: formic acid, PoA: propanoic acid, AA: acrylic acid, AcA: acetic acid.

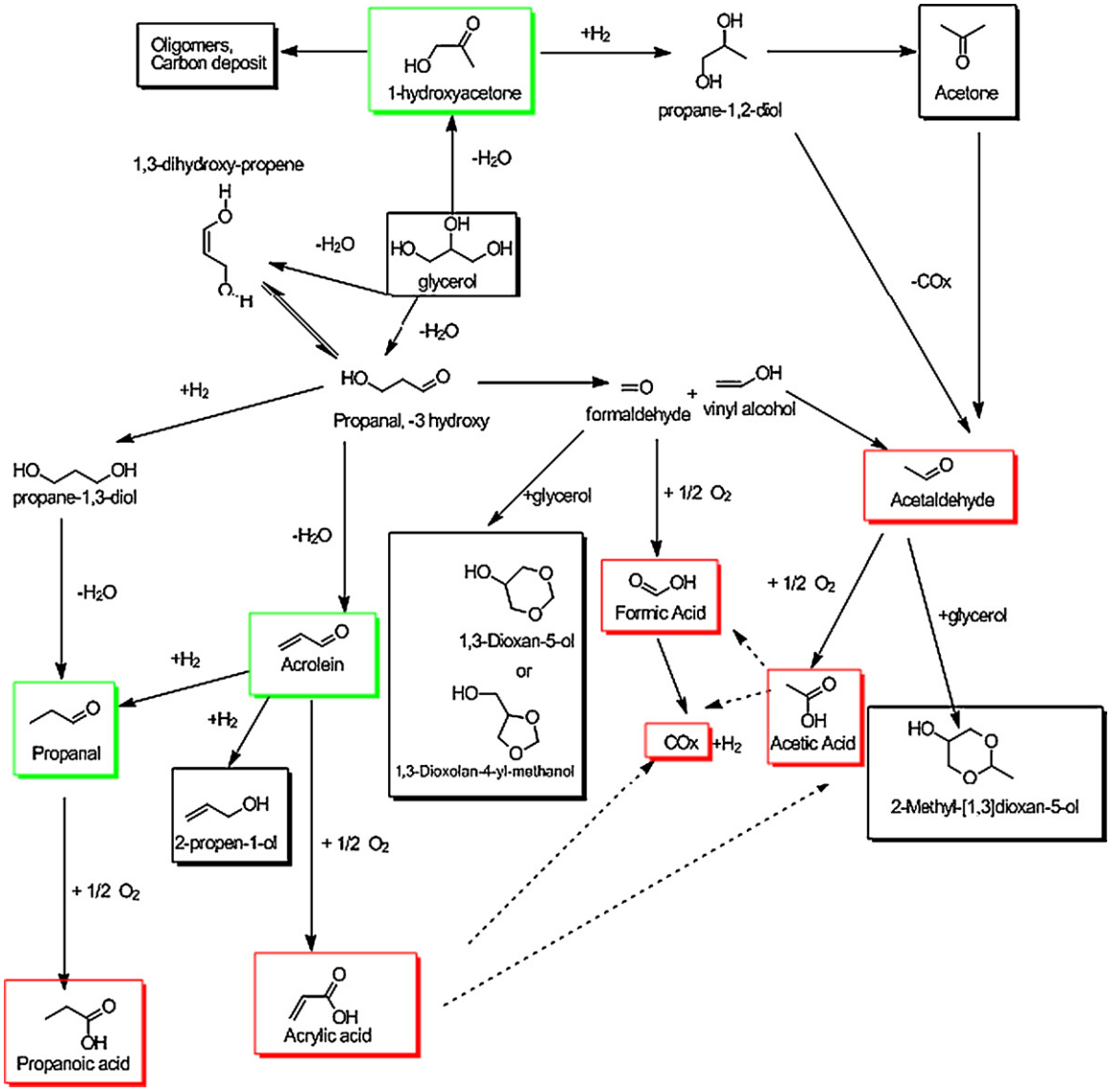

Fig. 7. Proposed mechanism of (oxy)dehydration of glycerol. Surrounded products were detected. Oxygen helps the formation of products in red on detriment of products in green. (For interpretation of the references to color in this figure legend, the reader is referred to the web version of the article.)

3.3. Reaction mechanism

Few mechanisms for the dehydration of glycerol were proposed in the literature. Based on these proposals and results obtained in this study with and without oxygen, we propose the following glycerol (oxy)dehydration mechanism (Fig. 7). For dehydration, all authors agree the first loss of water leading to 3-hydroxypropanal (not detected) and hydroxyacetone. 3-hydroxypropanal mainly leads to a second dehydration to form acrolein, the main observed product. Anyway, through retroaldol reaction, 3-hydroxypropanal can lead to acetaldehyde and formaldehyde. Acetaldehyde is always detected, formaldehyde not so much. In our case, formaldehyde can react with glycerol to form cyclic-ether products (Fig. 7) or with oxygen to form formic acid and CO_x. With deactivation, probably due to carbon deposit on the surface of the catalyst and modification of the active sites, preferred routes are changing, leading to hydroxyacetone, acetaldehyde and propanal.

In presence of oxygen, hydroxyacetone disappears on the benefit of acetaldehyde (FeP) and acetic acid (Mo/W–VO). Oxidation products such as formic acid, acetic acid, propanoic acid and CO_x, logically increase. Acrylic acid can be obtained if the catalyst is properly chosen.

4. Conclusions

(Oxy)dehydration of glycerol was studied with mixed oxide catalysts. Iron phosphate catalysts, weak solid acid, were active and selective to obtain acrolein. Best performances, in terms of yield in acrolein or stability, were obtained with well-crystallised $FePO_4$ prepared by hydrothermal synthesis with 100% conversion of glycerol and 92% selectivity in acrolein. However, deactivation occurred after 25 h. Use of oxygen could decrease the amount of carbon deposit and hydroxyacetone, but also amount in acrolein in aid of acetaldehyde, acetic acid and CO_x. $FePO_4$ catalysts could not oxidize acrolein in acrylic acid. Molybdenum (tungsten) vanadium based catalysts showed interesting results in the one-step oxydehydration of glycerol, leading to the highest yield (28.4%) in acrylic acid obtained in the literature up to now. However, yields in acetic acid were always high (23%) and deactivation was unfortunately also observed. New tungsten vanadium catalyst was hydrothermally synthesised and produced less by-products. Further work

will present a way to reduce the amount of acetic acid, by decreasing the surface acidity of the catalyst.

References

[1] G.W. Huber, S. Iborra, A. Corma, Chem. Rev. 106 (2006) 4044.
[2] A. Corma, S. Iborra, A. Velty, Chem. Rev. 107 (2007) 2411.
[3] S.E. Koonin, Science 311 (2006) 435.
[4] D.L. Klass, Biomass for renewable Energy, Fuels and Chemicals, Academic Press, San Diego, 1998, 1.
[5] G.W. Keulks, L.D. Krenzke, T.M. Notermann, Adv. Catal. 27 (1978) 183.
[6] Schering-Kahlbaum AG, FR 695931 (1930).
[7] E. Tsukuda, S. Sato, R. Takahashi, T. Sodesawa, Catal. Commun. 8 (2007) 1349.
[8] S.-H. Chai, H.-P. Wang, Y. Liang, B.-Q. Xu, J. Catal. 250 (2007) 342.
[9] S.-H. Chai, H.-P. Wang, Y. Liang, B.-Q. Xu, Green Chem. 9 (2007) 1130.
[10] A. Corma, G.W. Huber, L. Sauvanaud, P. O'Connor, J. Catal. 257 (2008) 163.
[11] H. Atia, U. Armbruster, A. Martin, J. Catal. 258 (2008) 71.
[12] Q. Liu, Z. Zhang, Y. Du, J. Li, X. Yang, Catal. Lett. 127 (2009) 419.
[13] A. Ulgen, W. Hoelderich, Catal. Lett. 131 (2009) 122.
[14] W. Suprun, M. Lutecki, T. Haber, H. Papp, J. Mol. Catal. A: Chem. 309 (2009) 71.
[15] B. Katryniok, S. Paul, M. Capron, F. Dumeignil, ChemSusChem 2 (8) (2009) 719.
[16] J.-L. Dubois, C. Duquenne, W. Hoelderich, J. Kervennal, WO 2006087084 (2006).
[17] J.-L. Dubois, C. Duquenne, WO2006087083 (2006).
[18] F. Wang, J.-L. Dubois, W. Ueda, J. Catal. 268 (2009) 260.
[19] E. Muneyama, A. Kunishige, K. Ohdan, M. Ai, J. Mol. Catal. 89 (1994) 371.
[20] M. Ai, J. Mol. Catal. 114 (1996) 3.
[21] M. Ai, K. Odhan, Appl. Catal. 180 (1999) 47.
[22] J.-M.M. Millet, Catal. Rev. -Sci. Eng. 40 (1998) 1.
[23] D. Vitry, Y. Morikawa, J.L. Dubois, W. Ueda, Appl. Catal. 251 (2003) 411.
[24] T. Katou, D. Vitry, W. Ueda, Catal. Today 91–92 (2004) 237.
[25] W. Ueda, D. Vitry, T. Katou, Catal. Today 96 (2004) 205.
[26] W. Ueda, D. Vitry, T. Katou, Catal. Today 99 (2005) 43.
[27] M. Sadakane, K. Kodato, T. Kuranishi, Y. Nodasaka, K. Sagawara, N. Sakaguchi, T. Nagai, Y. Matsui, W. Ueda, Angew. Chem. Int. Ed. 47 (2008) 2493.
[28] Y. Song, P.Y. Zavalij, M. Suzuki, M.S. Whittingham, Inorg. Chem. 41 (2002) 5778.
[29] J.M.M. Millet, M. Baca, A. Pigamo, D. Vitry, W. Ueda, J.L. Dubois, Appl. Catal. 244 (2003) 359.
[30] M.R. Nimlos, S.J. Blanksby, X. Qian, M.E. Himmel, D.K. Johnson, J. Phys. Chem. A 110 (2006) 6145.